ELSEVIER

Silicon adatoms on the Si(1 1 1)5 × 2–Au surface

A. Kirakosian [a], J.N. Crain [a], J.-L. Lin [a], J.L. McChesney [a], D.Y. Petrovykh [a], F.J. Himpsel [a], R. Bennewitz [b,*]

[a] *Department of Physics, UW-Madison, 1150 University Ave., Madison, WI 53706, USA*
[b] *Department of Physics and Astronomy, University of Basel, 4056 Basel, Switzerland*

Abstract

Scanning tunneling microscopy images of the Si(1 1 1)5 × 2–Au surfaces exhibit irregularly distributed protrusions of atomic size. They are identified as silicon adatoms by evaporating small amounts of silicon and gold onto the reconstructed surface. While extra silicon increases the density of protrusions, extra gold transforms the reconstruction partially into a Si(1 1 1)$\sqrt{3} \times \sqrt{3}$ reconstruction.
© 2003 Elsevier Science B.V. All rights reserved.

1. Introduction

A variety of surface reconstructions can be induced by low coverages of metals on the Si(1 1 1) surface. In many cases, the threefold symmetry of the surface is spontaneously broken and one-dimensional atomic arrangements are found [1–4]. Chains of metal atoms formed in this way have attracted a lot of attention, as they may constitute the geometric prerequisite for a one-dimensional electron gas. Particular attention has been given to detect the varying dimensionality in the electronic structure. For various reconstructions of Au on Si(1 1 1) the electronic structure has been investigated by means of angle-resolved photoelectron spectroscopy [2–4]. This technique is able to reveal the complete set of quantum numbers for one- and two-dimensional electrons, particularly the energy and the momentum parallel to the surface. Metal chain structures on vicinal Si(1 1 1) display interesting electronic features [1], among them charge density waves, the Peierls gap, bands with mixed dimensionality, and possibly spin–charge separation in a Luttinger liquid.

To allow for studies of one-dimensional electronic states it is necessary to align the one-dimensional chains to one of the three possible domains. This is achieved by using vicinal Si(1 1 1) which exhibits a regular step pattern [5] and aligns the atomic chains parallel to the step edges. Other examples of such one-dimensional reconstructions are Si(1 1 1)3 × 1–Ag [1], Si(1 1 1)3 × 1–Ca [6], and Si(1 1 1)5 × 2–Gd [7]. The latter could be of particular interest due to the strong magnetic moment of Gd atoms whose coupling along the one-dimensional chains has yet to be explored.

* Corresponding author. Address: Institut für Physik, Universität Basel, Klingelbergstr. 82, 4056 Basel, Switzerland. Tel.: +41-61-267-3725; fax: +41-61-267-3784/3824.
E-mail address: roland.bennewitz@unibas.ch (R. Bennewitz).

In this contribution we focus on the $Si(1\,1\,1)5 \times 2$–Au surface and discuss a peculiar structural feature of this surface, i.e. protrusions on top of the chains (Fig. 1) which form a lattice gas in a frozen state at room temperature. We identify them as single silicon atoms using scanning tunneling microscopy (STM) combined with controlled evaporation of Si and Au.

The structure of $Si(1\,1\,1)5 \times 2$–Au has been studied by a number of research groups employing a variety of methods [8–17]. The typical appearance of the $Si(1\,1\,1)5 \times 2$ in STM images consists of double rows with a distance of five lattice constants. The periodicity along the rows is two lattice constants. However, the phase is not correlated between adjacent unit cells, giving rise to long half order streaks in low energy electron diffraction (LEED). Protrusions show up on specific sites of the 5×2 structure with a preferred spacing of four lattice constants along the chains. They randomly occupy half of the available 5×4 sites, corresponding to a coverage of 1/40 of a $Si(1\,1\,1)$ layer.

Early STM reports [9,12] attributed the protrusions to Au adatoms based on the finding that the saturation coverage for $Si(1\,1\,1)5 \times 2$–Au is 0.443 ML [8], i.e. about $1/(5 \times 4)$ ML more than the four Au atoms per (5×2)-cell expected for the double row structure. Baski et al. have questioned this attribution with the observation that the density of protrusions does not depend on the Au coverage [10]. In fact, we find a slight decrease of the density for a gold coverage above the optimum coverage for $Si(1\,1\,1)5 \times 2$–Au which provides even stronger evidence against gold atoms.

While the appearance of the protrusions in STM images does not depend significantly on the bias voltage, the underlying row structure does, indicating that imaging of the row structure strongly involves the electronic structure of this reconstruction. O'Mahoney et al. counted eight distinguishable features in a unit cell and concluded that features cannot be related to individual gold atoms [11]. Comparing Fig. 1(a) and (b) we suggest that not only the bias voltage but also the atomic configuration of the tip determines the appearance of the row structure. While Fig. 1(a) resembles the asymmetric features reported by O'Mahoney, Fig. 1(b) exhibits perfect zig-zag rows of round features. Please note that the positions of these round features do not necessarily indicate positions of Au atoms. Considering the different appearances of the row structure in different STM images it appears inadequate to make an assignment of STM features to certain features of the structure. To better interpret STM images it would be desirable to know the surface density of states in structural
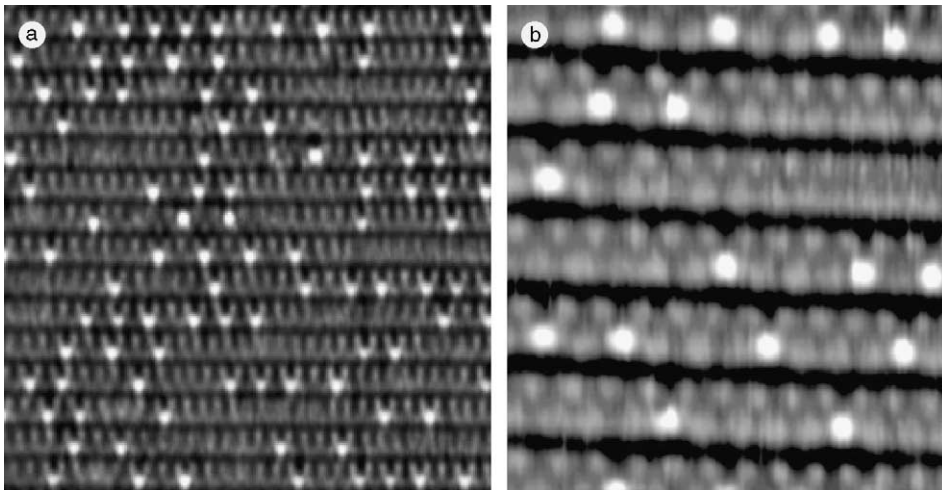

Fig. 1. STM images of the $Si(1\,1\,1)5 \times 2$–Au surface. The sample bias voltage, tunneling current, and frame size are (a) −2.2 V, 0.2 nA, 25×25 nm^2, (b) −1.5 V, 0.2 nA, 9×9 nm^2. The actual appearance of the row structure depends on the tip condition and on the sample bias voltage.

models like that of Marks and Plass. This model contains two lines of gold atoms residing in the heavily rearranged Si surface and is based on transmission electron microscopy and heavy-atom holography [13].

2. Experimental

Vicinal Si(1 1 1) surfaces tilted by 1° towards the [1 $\bar{1}$ 2] azimuth are used as substrates in this study. By applying a standard annealing sequence, a regular pattern of straight steps and large domains of the 7×7 reconstruction are obtained [5]. Gold is evaporated from a molybdenum wire basket with a typical rate of 0.015 ML/s with the sample held at a temperature of 650 °C. Subsequently, the sample is annealed to 950 °C. The sample can then be repeatedly cleaned by annealing to 850 °C. The Au coverage for a perfect Si(1 1 1)5×2–Au surface can be accurately calibrated by means of the phase diagram of Au-induced surface reconstructions. At coverages below the optimum, patches of Si(1 1 1)7×7 coexist with the 5×2 structure (Fig. 2(a)), while patches of the $\sqrt{3} \times \sqrt{3}$ appear when the coverage is too high (Fig. 2(b)). Silicon is evaporated from a wafer heated by direct current at a rate of 0.004% of a monolayer per second. Coverage calibration is done using LEED and STM. A typical coverage calibration is obtained using an STM image like in Fig. 3, where extra Si atoms are deposited at room temperature atop Si(1 1 1)5×2–Au. Since Si adatoms do not diffuse
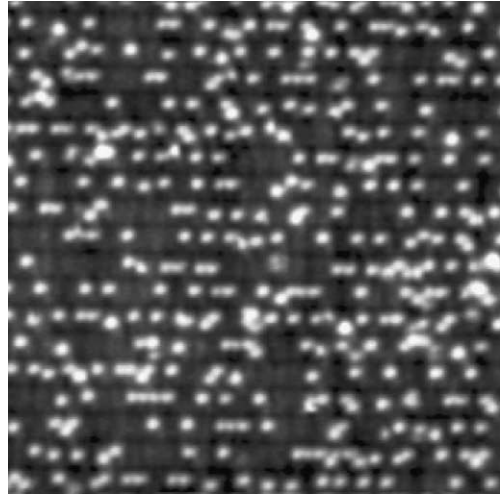

Fig. 3. Coverage calibration using a STM image of Si(1 1 1)5×2–Au after deposition of extra Si at room temperature (-2 V, 0.2 nA, 30×30 nm^2). Lack of diffusion at room temperature allows the counting of individual adatoms, which yields a coverage of 0.048 ML, or 0.023 ML more than the equilibrium coverage of 0.025 ML.

at room temperature they can be counted individually. Such a count for Fig. 3 yields an adatom coverage of 0.048 ML, which is 0.023 ML over the equilibrium 0.025 ML coverage. All STM images are recorded in situ at room temperature.

3. Results and discussion

In all STM images recorded on the Si(1 1 1) 5×2–Au surface we find characteristic irregularly
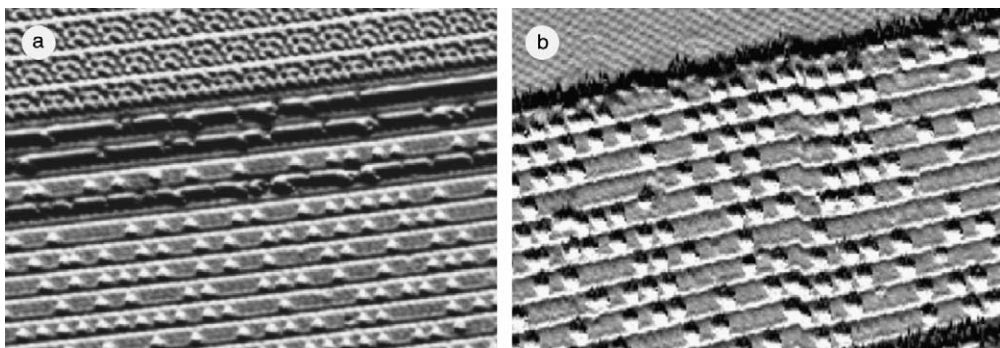

Fig. 2. Images of the Si(1 1 1) surface with Au coverage below (a) and above (b) the optimum coverage for Si(1 1 1)5×2–Au. In (a) the Si(1 1 1)5×2–Au structure coexists with Si(1 1 1)7×7, in (b) with Si(1 1 1)$\sqrt{3} \times \sqrt{3}$–Au (-1 V, 0.5 nA), (a) 39×28 nm^2, for (b) 39×23 nm^2. In this figure, the derivative of the topography is shown in order to clearly visualize atomic-sized features in the presence of a step.

distributed protrusions spaced by multiples of two lattice constants along the rows. Since their basic appearance is independent of the tunneling conditions, we conclude that these protrusions indicate the location of adatoms rather than features in the density of electronic states. Note that these adatoms are not the same as the Si adatoms on the clean Si(1 1 1)7 × 7 surface, which appear brighter at positive sample bias. For well-annealed Si(1 1 1)5 × 2–Au surfaces with optimum stoichiometry we always find the average filling of the 5 × 4 cells within the Si(1 1 1)5 × 2–Au structure to be 50%. This density drops to 35–40%, when the Au coverage is above the optimum and Si(1 1 1)$\sqrt{3} \times \sqrt{3}$–Au patches are formed (Fig. 2(b)).

In Fig. 4, we present STM images of the Si(1 1 1)5 × 2–Au surface before (a) and after (b) evaporating a small amount of silicon onto the surface at 300 °C. The only effect of depositing extra silicon is an increase of the number of protrusions. In Fig. 4(b), about 90% of the possible sites for protrusions are filled after the evaporation. The identical appearance of the additional protrusions leads us to conclude that the protrusions represent silicon adatoms on the Si(1 1 1)5× 2–Au surface. After evaporation of 0.04 ML of silicon onto Si(1 1 1)5 × 2–Au at 400 °C (Fig. 5) the number of silicon atoms exceeds the available
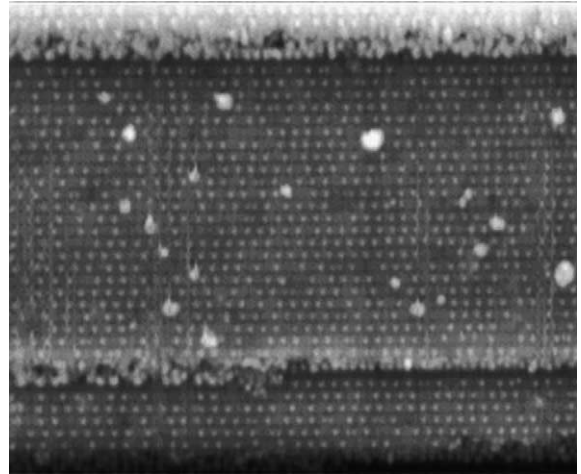

Fig. 5. STM image of Si(1 1 1)5 × 2–Au after evaporation of 0.04 ML Si at 400 °C. The density of silicon adatoms exceeds the density of available adatom sites and leads to the formation of clusters at steps and on the wide terrace (−1.5 V, 0.4 nA, 77 × 64 nm^2).

sites for adatoms by about 60%. The excess silicon starts to form small clusters at the adjacent steps as well as on the wider terraces. Narrow terraces are devoid of the clusters, indicating that adatoms attach to the nearest step edge before finding a defect or an adatom partner for nucleation on the terrace. Furthermore, the filling of the protrusion sites is no longer complete. After annealing to
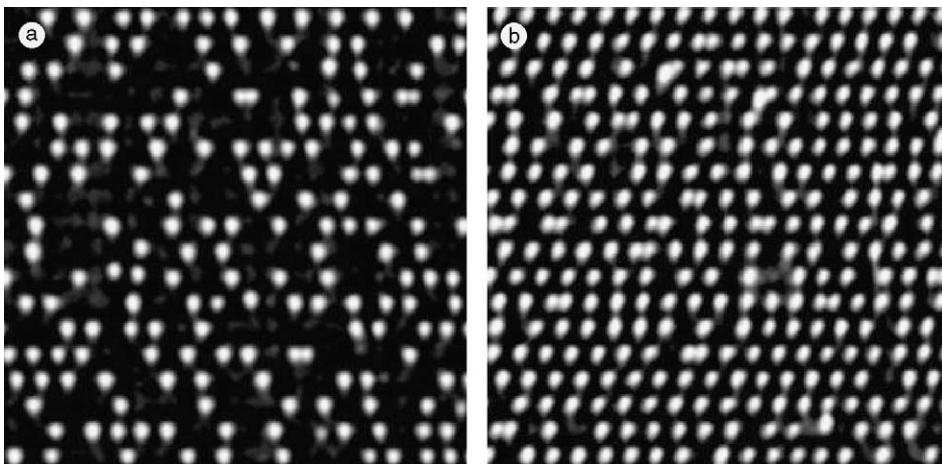

Fig. 4. STM images of (a) Si(1 1 1)5 × 2–Au in thermal equilibrium and (b) after additional evaporation of 0.025 ML silicon at 300 °C. About 90% of all 5 × 4-cells are filled (−2 V, 0.2 nA, 30 × 30 nm^2).

850 °C, the extra filling of protrusion sites disappears and the equilibrium filling of 50% of the possible sites is regained.

In a complementary experiment we have deposited fractions of a monolayer of Au at room temperature onto Si(1 1 1)5 × 2–Au surfaces. A typical result is given in Fig. 6. The extra deposition of 0.08 ML of Au at 300 °C and a post-anneal at 400 °C result in the formation of extra patches of Si(1 1 1)$\sqrt{3} \times \sqrt{3}$–Au. The $\sqrt{3} \times \sqrt{3}$ phase is not resolved under the given tunneling conditions, but its presence is confirmed by the observation of extra $\sqrt{3} \times \sqrt{3}$ diffraction spots in LEED. Only 5 × 2 diffraction spots are observed prior to the deposition of extra gold. The density of the protrusions in Fig. 6 remains close to the original 50%, but it drops to 35–40% upon annealing to 850 °C, as shown in Fig. 2(b).

Our assignment of the protrusions seen in STM as silicon adatoms is in agreement with other experimental results. Hill and McLean have found a strong signature of silicon adatoms in inverse photoemission spectra [17]. Comparing the emission yield with that of Si(1 1 1)7 × 7 the authors expected an uneven number of adatoms per un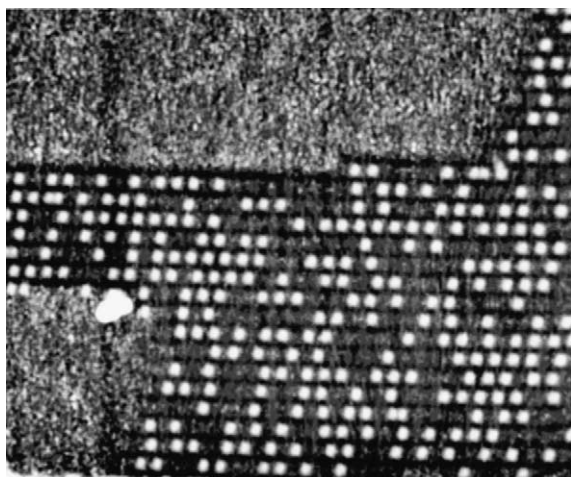it cell, which could be explained by the irregularly occupied adatom sites. Furthermore, we have successfully removed single protrusions in STM manipulation experiments using procedures that are well established for removal of adatoms from the Si(1 1 1)7 × 7 surface [18].

An understanding of the equilibrium occupation of 50% of the available 5 × 4 cells by adatoms will require a structural model which explains the function of the adatoms. How silicon adatoms contribute to the stabilization of the Si(1 1 1)5 × 2–Au reconstruction remains an open question. It should be noted that such features are not observed on other metal-induced one-dimensional reconstructions of Si(1 1 1), with the exception of Si(5 5 7)–Au [2,4]. Three findings are to be taken into consideration, the random distribution of the adatoms, the mobility of the adatoms along the chains at elevated temperatures found by Hasegawa and Hosoki [12], and the ability of any 5 × 4 cell to host a silicon adatom found in our study by silicon evaporation. All 5 × 4 cells are equivalent and provide the reference points for a lattice gas of adatoms. The important parameter appears to be the density of adatoms. Their function could be related to charge transfer. An indication of such a surface doping mechanism is the reduced height of those few protrusion which occupy adjacent 5 × 2 cells (about 4% in Fig. 4(a) and compare Fig. 6 in Ref. [12]).

4. Conclusion

The protrusions found in STM images of the Si(1 1 1)5 × 2–Au reconstruction have been identified as Si adatoms by controlled evaporation of Si and Au onto the surface. Si evaporation fills open sites on the surface with such protrusions, while Au evaporation results in the formation of patches of Si(1 1 1)$\sqrt{3} \times \sqrt{3}$–Au which take up the extra Au. The Si adatoms can be used to demonstrate data storage at the atomic limit, as discussed elsewhere [18]. Basically, a 1 is encoded by the presence of an adatom, a 0 by its absence. Filling the adatom sites by Si evaporation preformats the memory with ones, and zeros can be written by removing single adatoms with the STM tip.

Fig. 6. STM image of a Si(1 1 1)5 × 2–Au surface after evaporation of 0.08 ML Au at 300 °C and a post-anneal at 400 °C. The grainy areas are patches of Si(1 1 1)$\sqrt{3} \times \sqrt{3}$ as revealed by STM imaging with different parameters and by LEED (−2 V, 0.5 nA, 50 × 42 nm^2).

Acknowledgements

References

[1] F.J. Himpsel, K.N. Altmann, R. Bennewitz, J.N. Crain, A. Kirakosian, J.-L. Lin, J.L. McChesney, J. Phys.: Condens. Matter 13 (2001) 11097.

[2] K.N. Altmann, J.N. Crain, A. Kirakosian, J.-L. Lin, D.Y. Petrovykh, F.J. Himpsel, Phys. Rev. B 64 (2001) 035406.

[3] P. Segovia, D. Purdie, M. Hengsberger, Y. Baer, Nature (London) 402 (1999) 504.

[4] R. Losio, K.N. Altmann, A. Kirakosian, J.-L. Lin, D.Y. Petrovykh, F.J. Himpsel, Phys. Rev. Lett. 86 (2001) 4632.

[5] J. Viernow, J.-L. Lin, D.Y. Petrovykh, F.M. Leibsle, F.K. Men, F.J. Himpsel, Appl. Phys. Lett. 72 (1998) 948.

[6] D.Y. Petrovykh, K.N. Altmann, J.-L. Lin, F.J. Himpsel, F.M. Leibsle, Surf. Sci. 512 (2002) 269.

[7] A. Kirakosian, J.L. McChesney, R. Bennewitz, J.N. Crain, J.-L. Lin, F.J. Himpsel, Surf. Sci. 498 (2002) L109.

[8] W. Schwiech, E. Bauer, M. Mundschau, Surf. Sci. 253 (1991) 283.

[9] T. Hasegawa, K. Takata, S. Hosaka, S. Hosoki, J. Vac. Sci. Technol. A 8 (1990) 241.

[10] A.A. Baski, J. Nogami, C.F. Quate, Phys. Rev. B 41 (1990) R10247.

[11] J.D. O'Mahoney, J.F. McGilp, C.F.J. Flipse, P. Weightman, F.M. Leibsle, Phys. Rev. B 49 (1994) 2527.

[12] T. Hasegawa, S. Hosoki, Phys. Rev. B 54 (1996) 10300.

[13] L.D. Marks, R. Plass, Phys. Rev. Lett. 75 (1995) 2172.

[14] Ch. Champer, W. Moritz, H. Schulz, R. Feidenhans'l, M. Nielsen, F. Grey, R.L. Johnson, Phys. Rev. B 43 (1991) 12130.

[15] L. Seehofer, S. Huhs, G. Falkenberg, R.L. Johnson, Surf. Sci. 329 (1995) 157.

[16] L.M. Shibata, I. Sumita, M. Nakajima, Phys. Rev. B 57 (1998) 1626.

[17] I.G. Hills, A.B. McLean, Phys. Rev. B 55 (1997) 15664.

[18] R. Bennewitz, J.N. Crain, A. Kirakosian, J.-L. Lin, J.L. McChesney, D.Y. Petrovykh, F.J. Himpsel, Nanotechnology 13 (2002) 499.